Enantioselectivity of Adsorption Sites Created by Chiral 2-Butanol Adsorbed on Pt(111) Single-Crystal Surfaces

Ilkeun Lee and Francisco Zaera*

Department of Chemistry, University of California, Riverside, California 92521

Received: March 22, 2005; In Final Form: April 26, 2005

The adsorption and thermal chemistry of 2-butanol and propylene oxide, each individually and when coadsorbed together, were characterized on Pt(111) single-crystal surfaces by using temperature programmed desorption and reflection-adsorption infrared spectroscopies. The formation of chiral superstructures on the surface upon the deposition of submonolayer coverages of enantiopure 2-butoxide species, produced by thermal dehydrogenation of 2-butanol, was highlighted by their difference in behavior toward the adsorption of the two enantiomers of propylene oxide. It was found that a significant enhancement in adsorption is possible on surfaces with the same chirality of the probe molecule, that is, for (*R*)-propylene oxide adsorption on (*R*)-2-butoxide layers and for (*S*)-propylene oxide adsorption on (*S*)-2-butoxide layers. The propylene oxide probe was found to also adsorb with the ring closer to the surface in those cases. Finally, less butoxide decomposition is seen at higher temperatures from the homochiral pairing, presumably because the coadsorbed propylene oxide forces the alkoxides into a more compact and better packed structure on the surface.

1. Introduction

The possibility of bestowing chiral properties to achiral solid surfaces by adsorption of chiral molecules has been explored in recent years in connection with biomineralization,[1] separation of racemic mixtures,[2] self-assembly,[3,4] and electrochemistry,[5] among others. In heterogeneous catalysis in particular it has been shown that the adsorption of chiral modifiers can be used to make achiral solid catalysts enantioselective.[6] Perhaps the most successful example of this application has been the use of chiral cinchona modifiers to impart chirality to platinum and palladium hydrogenation catalysts for the conversion of α-keto esters to α-hydroxo esters.[7−10] Indeed, enantioselectivities above 95% of enantiomeric excess (e.e.), higher than with homogeneous catalysts, have been obtained in selected cases.[11] It has been suggested that this enantioselectivity is induced by (1) the formation of a complex between individual cinchona molecules and the reactant and (2) its adsorption in a particular geometry on the surface so hydrogenation is forced selectively on one side of the carbonyl plane.[12,13] The details of the mechanisms for this reaction are still far from understood, but recent surface characterization experiments by us[14−18] and others[19,20] have indicated that the performance of the cinchona-modified catalysts is mostly controlled by the characteristics of the adsorption of the chiral modifier.

There have also been reports of a second example of chiral-modified catalysts for the enantioselective hydrogenation of *β*-keto esters,[21−23] specifically of the use of tartaric acid to modify nickel surfaces. Given that tartaric acid is a relatively simple molecule, it is less likely for this chiral modification to rely on the type of one-to-one interactions with the reactant invoked in the cinchona/platinum system. Instead, it has been proposed that perhaps the chiral modifier adsorbs on the surface in an ordered suprastructure containing void spaces with chiral properties in terms of their ability to adsorb other chiral molecules.[24] Ordered structures with chiral empty sites have indeed been identified on copper surfaces by using a combination of surface-sensitive techniques, including scanning tunneling microscopy (STM), low-energy electron diffraction (LEED), and reflection−absorption infrared spectroscopy (RAIRS).[25,26] Unfortunately, further work has shown that nickel single-crystal surfaces are less able to facilitate the formation of such stable ordered layers.[27,28] In a separate study, Tysoe et al. have proven that enantiopure 2-butoxide layers adsorbed on Pd(111) surfaces leave void surface sites with enantiopreference for the adsorption of homochiral propylene oxide molecules.[29] However, their more recent work with other chiral organic acids and amino acids has highlighted some surprising behavior, in particular because the extent of the chiral effect seems to vary in a nontrivial manner with the structure of the templating chiral modifier.[30] Both the differences in the behavior of tartaric acid on copper vs nickel and the variations in the extent of the chirality imparted by different modifiers on palladium pose fundamental questions on the role of the nature of the underlying surface in determining the formation of chiral suprastructures. To address this issue directly, here we report on titration experiments similar to those reported by Tysoe et al. but on Pt(111) single-crystal surfaces. Our temperature programmed desorption (TPD) and RAIRS data point to the formation of chiral adsorption sites upon deposition of 2-butoxide moieties on that metal substrate, but with a different level of enantioselectivity toward the subsequent adsorption of enantiopure propylene oxide.

2. Experimental Section

All TPD and RAIRS experiments reported here were performed in a two-tier ultrahigh-vacuum chamber cryopumped to a base pressure below 8×10^{-11} Torr.[31,32] The main stage of this chamber is used for the TPD experiments, which are performed by using a computer-controlled quadrupole mass spectrometer (UTI 100C) with an extendible nose cone ended in a 5 mm diameter aperture which can be placed within 1 mm of the single crystal for the selective detection of molecules desorbing from the front surface of the crystal. A constant

* Corresponding author. E-mail: zaera@ucr.edu.

10.1021/jp051494v CCC: $30.25
Published on Web 06/10/2005

heating rate of 10 K/s was used in all TPD runs, and a bias of −100 V was applied to the crystal in order to avoid any chemistry induced by stray electrons from the ionizers of the ion gauge or the mass spectrometer.[33] The mass spectrometer is interfaced to a personal computer in order to record the signals of up to 15 different ions during a single TPD experiment.

A second, smaller stage accessible using a long-travel manipulator is employed for the RAIRS experiments. The infrared beam from a FT-IR spectrometer (Bruker Equinox 55) is passed through a polarizer and focused through a NaCl window onto the platinum crystal at a grazing (∼85°) incidence. The reflected beam that escapes from the ultrahigh-vacuum chamber through a second NaCl window is then refocused onto a narrow-band mercury−cadmium−telluride (MCT) detector. The entire beam path is enclosed in a sealed box purged with dry air purified using a scrubber (Balston 75-60) for CO_2 and water removal. All spectra were taken at a resolution of 4 cm^{-1} by averaging over 2000 scans, a process that takes about 4 min/experiment, and were ratioed against spectra from the clean surface acquired before gas dosing. Both the condition of the sample and the infrared beam alignment were checked routinely by comparing infrared spectra for a saturation coverage of CO with those reported in the literature.[34,35]

The platinum (111) single crystal, a disk 8 mm in diameter and 2 mm in thickness, was mounted on the sample holder by spot-welding it to two tantalum wires attached to two copper electrical feed-throughs. With this arrangement, it is possible to cool the sample to below 80 K using a continuous flow of liquid nitrogen through hollow tubes connected to the non-vacuum side of the copper feed-throughs, and also to heat the crystal resistively to up to 1100 K. The surface temperature is measured with a chromel−alumel thermocouple spot-welded to the side of the crystal and set to within ±1 K of any given value by using a homemade temperature controller also employed to ramp the temperature linearly for the TPD experiments. The sample was regularly cleaned by cycles of oxidation in 5×10^{-7} Torr of oxygen at 700 K and annealing under vacuum at 1100 K. Ar^+ ion sputtering followed by annealing at 1100 K was used as needed but sparingly to minimize the creation of surface detects.

All (*R*)- and (*S*)-propylene oxide (ProO, 99% purity) and (*R*)- and (*S*)-2-butanol (2-ButOH, 99% purity) enantiomers were purchased from Aldrich and used as supplied after a series of freeze−pump−thaw vacuum distillations. Their purities were checked frequently in situ in the main ultrahigh-vacuum chamber by mass spectrometry. Dosing was achieved by leaking controlled amounts of the vapors into the vacuum chamber. They were carried out at 80 K unless otherwise indicated, and reported in langmuirs (1 L ≡ 10^{-6} Torr·s), not corrected for differences in ion gauge sensitivities.

3. Results

3.1. Adsorption of 2-Butanol. The uptake of (*S*)-2-butanol on Pt(111) at 100 K was first characterized by RAIRS. The data are reported in Figure 1, and the vibrational assignment, in Table 1.[29,36] The spectra for the multilayer agree well with those reported for the gas-phase alcohol.[37] Notice in particular the broad bands around 1060−1200 and 3200−3800 cm^{-1}, corresponding to the in-plane deformation, δ_{ip}(OH), and stretching, ν(OH), modes of hydrogen-bonded OH moieties, respectively. Given that those absorptions start to develop around 1.5 langmuirs, that exposure is taken here as the onset for multilayer adsorption. On the other hand, the spectrum for 1.0 langmuir, which corresponds approximately to monolayer saturation,

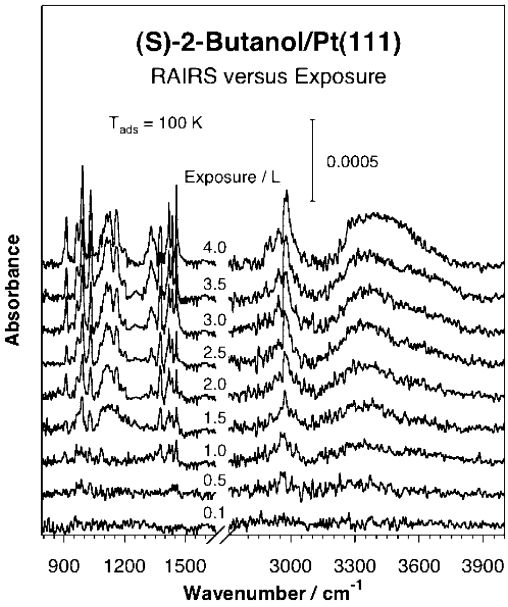

Figure 1. Reflection-absorption infrared spectra (RAIRS) as a function of exposure for (*S*)-2-butanol adsorbed on a Pt(111) single-crystal surface at 100 K.

shows some unique features. In particular, the peak corresponding to the stretching of the C−O bond, ν(CO), shifts from 1112 to 1088 cm^{-1}, indicating that the adsorption of the alcohol takes place via its hydroxyl group. In addition, the features for the in-plane O−H deformation, δ_{ip}(OH), and C−H deformation, δ(CH), at 1158 and 1331 cm^{-1} respectively, are no longer visible, most likely because those bonds are oriented close to parallel to the surface.[38−40] All this suggests that the molecule binds to the platinum surface through its oxygen atom and adopts a geometry with the C−O bond approximately perpendicular to the surface.

Figure 2 reports the TPD data obtained for 2.0 langmuir of (*S*)-2-butanol adsorbed on Pt(111) at 100 K. Because of the complexity of the chemistry involved, a number of ion fragments were followed. A small amount of hydrogen is produced, as seen in a broad desorption feature with onset at 300 K (data not shown). A spike is also seen in some traces around 170 K because of 2-butanol multilayer desorption. Additional products are detected in two broad temperature ranges, around 220−300 and about 300−360 K. In fact several overlapping peaks can be identified in each of those regions. Specifically, the signals for 45 and 59 amu, which peak about 260 K, correspond mostly to molecular 2-butanol desorption, while those for 43, 57, and 72 amu with maxima around 270 K can be identified with butanone. These assignments are consistent with the features seen for the other masses, which follow the reported cracking patterns of the individual products.[41] The conversion of alcohols to ketones, which takes place by dehydrogenation of the hydroxyl group followed by β-hydride elimination from the resulting surface alkoxide, has been observed with other alcohols in the past.[42−46] In terms of the high-temperature chemistry, again, at least two contributions can be identified in the TPD data of Figure 2, the 320 K peaks in the 41 and 42 amu traces likely due to butylene oxide desorption and the 325 K features for 29, 43, and 72 amu, which probably correspond to butanal. In addition, the TPD trace for 27 amu peaks at a slightly higher temperature, about 330 K, and therefore must include the production of another product, possibly ethylene. Finally, the traces for both 30 and 58 amu display an early

TABLE 1: Vibrational Assignment of RAIRS Frequencies (cm^{-1}) for (*S*)-2-Butanol Adsorbed on Pt(111)

	2-butanol/Pt(111)			2-butanol/Pd(111)[29]		
assignment[a]	multilayer	monolayer	2-butoxide	multilayer	monolayer	2-butoxide
ν(OH)	3130−3380	3100−3500				
$\nu_a(CH_3)$	2963	2953	2960	2968		2961
$\nu_a(CH_2)$	2925	2922	2915	2934, 2924	2937	2934
$\nu_s(CH_3)$, ν(CH)	2885	2877	2879	2878	2878, 2870	2870
$\delta_a(CH_3)$	1436, 1457	1435, 1455	1453, 1462	1466, 1458	1452	1449
$\gamma(CH_2)$	1419	1419		1418	1400	
$\delta_s(CH_3)$	1377	1377	1380	1375	1377	1379
δ(CH)	1331			1337, 1279		
δ_{ip}(OH)	1158			1163	1153	
ν(CC), $\rho(CH_3)$	1129		1142	1128	1123	
ν(CO)	1112	1088	1084	1111		
ν(CC), $\rho(CH_3)$	1032	1025		1034	1026	1026
$\rho(CH_3)$	993	985	991	993	989	989
$\rho(CH_3)$	964	960	967	966		
$\rho(CH_2)$	912	903		914	897	885

[a] ν = stretching, δ = deformation, γ = scissoring, ρ = rocking, s = symmetric, a = asymmetric, and ip = in plane.

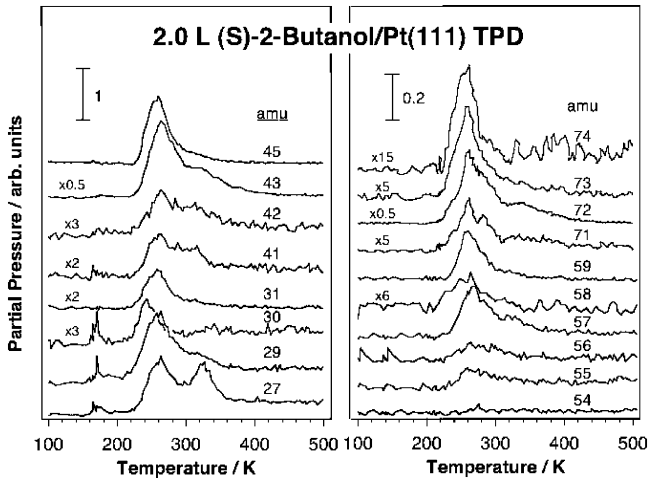

Figure 2. Temperature programmed desorption (TPD) data for 2.0 langmuirs of (*S*)-2-butanol adsorbed on Pt(111) at 100 K. Traces are reported for 18 different masses, recorded in three different experiments, to help with the identification of the desorbing species.

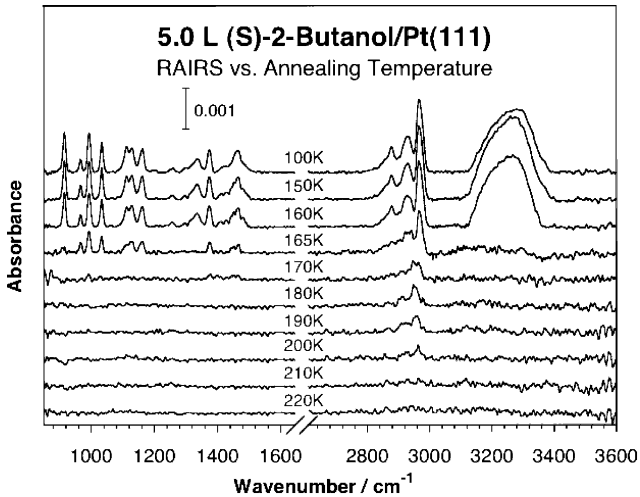

Figure 3. RAIRS versus annealing temperature for 5.0 langmuirs of (*S*)-2-butanol adsorbed on Pt(111). Multilayer desorption is evidenced around 165 K by the disappearance of the hydrogen-bonding broad bands around 1480 and 3250 cm^{-1}. The spectra in the 170−200 K range are identified with a 2-butoxide surface species.

feature about 240 K, perhaps because of the production of small amounts of ethane and propanal.

The TPD data in Figure 2 provide information about the products that desorb from the surface upon thermal activation of the adsorbates, but cannot be used to identify earlier surface reactions. For that we turn to the RAIRS annealing sequence for 5.0 langmuir of (*S*)-2-butanol on Pt(111) reported in Figure 3. There it is seen that the initial butanol multilayer desorbs around 165 K, as evidenced primarily by the disappearance of the broad features corresponding to the ν(OH) and δ_{ip}(OH) hydrogen-bonded vibrational modes. On the other hand, that spectrum still retains most of the original peaks of the multilayer (except for the intensity associated with hydrogen bonding), and therefore is likely to correspond to a 2-butanol monolayer. By 170 K, however, clear changes are observed, and only the two asymmetric C−H stretching modes, $\nu_a(CH_3)$ and $\nu_a(CH_2)$, are still easily seen, at 2960 and 2915 cm^{-1}, respectively, although a few weak peaks are also barely seen at 1462, 1453, 1380, 1142, 1086, and 991 cm^{-1}. Clearly, between 170 and 200 K a new species forms on the surface, with frequencies for the asymmetric C−H stretches red-shifted from those observed in the butanol, and the C−O stretch also shifted from 1188 to 1084 cm^{-1} (Table 1). Based on the similar behavior reported for 2-propanol on Ni(100),[46] this new species is identified here as surface 2-butoxide. Finally, the butoxide reacts further around 210 K, and by 220 K there are no discernible features in the IR data. This agrees well with the TPD data in Figure 2.

3.2. Adsorption of Propylene Oxide. Figure 4 displays infrared spectra for the uptake of (*R*)-propylene oxide on Pt-(111) at 100 K. The corresponding vibrational assignment for the most relevant peaks, made with the aid of previous data for the liquid and vapor of the pure compound[47] as well as for propylene oxide adsorbed on Pd(111),[29] is provided in Table 2. Roughly, three coverage regimes can be identified in this figure, namely: (1) exposures of 2.0 langmuirs or lower, which, based on the accompanying TPD data (Figure 5), is identified with the monolayer, (2) doses between 3.0 and 5.0 L, most likely corresponding to the buildup of a second layer, and (3) doses above 5.0 L, which reflect multilayer condensation. The latter displays a number of sharp peaks easily identified with the pure compound. The traces for the monolayer, on the other hand, only show peaks for a few selected modes, at 1401, 1020, 942, 890, and 822 cm^{-1}. Notice for instance the absence of any significant signal for the methyl symmetric deformation, $\delta_s(CH_3)$, and ring-methyl stretching, ν(ring-CH_3), modes, at 1369 and 1115 cm^{-1} respectively. This contrasts with the clear peak seen for the methyl rocking, $\rho(CH_3)$, at 942 cm^{-1}. On the basis of the RAIRS surface selection rule that applies to metal

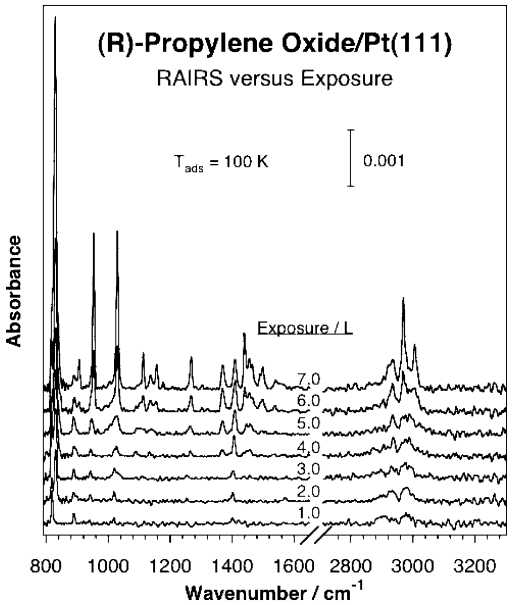

Figure 4. RAIRS data as a function of exposure for (*R*)-propylene oxide adsorbed on a Pt(111) single-crystal surface at 100 K. The spectra for the monolayer, for exposures below 2.0 langmuirs, display only a selected number of vibrations, many of which are red-shifted significantly from the values seen in the multilayer.

TABLE 2: Vibrational Assignments of RAIRS Frequencies (cm^{-1}) for Propylene Oxide Adsorbed on Pt(111)

	propylene oxide/Pt(111)		propylene oxide/Pd(111)[29]	
assignment[a]	multilayer	monolayer	multilayer	monolayer
$\nu_a(CH_3)$	2970	2978	2965	
$\nu_a(CH_2)$	2935	2931	2930	
$\delta_a(CH_3)$	1440, 1457	1441, 1458	1456	1441
$\gamma(CH_2)$	1410	1401	1409	1399
$\delta_s(CH_3)$	1369			
ν_a(COC)	1269	1255		
ν(ring-CH_3)	1115			
$\omega(CH_3)$	1030	1020	1026	1021
$\rho(CH_3)$	954	942	948	940
$\rho(CH_2)$	890, 906	890		
δ_{oop}(ring)	830	822	830	810

[a] ν = stretching, δ = deformation, γ = scissoring, ω = wagging, ρ = rocking, s = symmetric, a = asymmetric, and oop = out-of-plane.

surfaces,[38−40] those results can be interpreted as the consequence of the methyl moieties being oriented with their main axis close to parallel to the surface. On the other hand, the methylene scissoring mode, $\gamma(CH_2)$, is quite prominent at 1401 cm^{-1}, while the asymmetric ring stretching, ν(COC), at 1255 cm^{-1} is much weaker. Clearly, both the methylene−oxygen bond and the main plane of the methylene moiety must be at a significant angle from the surface plane. Also, the intense peaks detected for the methyl wagging, $\omega(CH_3)$, and methylene rocking, $\rho(CH_2)$, modes at 1020 and 890 cm^{-1} attest to a measurable tilt of the ring plane away from the surface normal. Finally, significant red shifts are observed for most of the vibrational modes involving the oxygen atom or the ring upon monolayer adsorption. All together, the data suggest that propylene oxide bonds through its oxygen atom and with the ring rotated so the methylene−oxygen bond is at an angle from the surface (the methylidyne−oxygen bond being closer to parallel to the surface) and its plane tilted from the surface normal.

The thermal chemistry of propylene oxide on Pt(111) was probed by TPD. Figure 5 displays the traces obtained for molecular (A, left) and hydrogen (B, right) desorption as a function of dose at 100 K for the case of the (*S*) enantiomer. Three main peaks populate sequentially in the molecular desorption data: (1) one at 220 K, which saturates after an exposure of approximately 0.1 langmuirs and is probably associated with surface defects, (2) a feature at 195 K, which starts growing about 0.5 langmuirs and saturates around 1.6 langmuirs with the completion of the monolayer, and (3) a peak at 145 K for the multilayers that grow beyond that point. Integration of the peak areas provides quantitative information on the uptake as a function of exposure (data not shown). It was found that the sticking probability of propylene oxide on the platinum surface changes from a value of approximately 0.4 monolayer/langmuir during the buildup of the first layer (one monolayer, corresponding to saturation coverage) to close to 1 monolayer/langmuir in the multilayer. Two additional observations stand in contrast between the TPD and RAIRS data in Figures 4 and 5: (1) the formation of a second layer distinct from the multilayer is clearly seen in the vibrational data, but it is not as obvious in the TPD results (although a shoulder is seen about 160−170 K in the traces for 1.8 and 2.0 langmuirs), and (2) while the TPD data suggest a sequential population of the first and subsequent layers, the RAIRS information indicates the start of the growth of the second layer before the monolayer is fully saturated. Notice in particular the growth of the 830 cm^{-1} signal due to the multilayer in the traces for the 1.0, 2.0, and 3.0 langmuirs exposures before saturation of the 822 cm^{-1} peak corresponding to the monolayer. It is possible that some three-dimensional deposition occurs at low temperatures, but that those layers are annealed and flatten out as the temperature of the surface is increased during the TPD experiments.

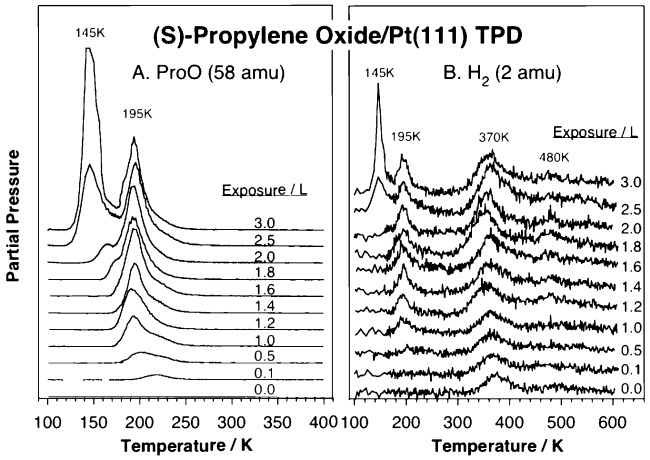

Figure 5. Molecular (58 amu, A) and hydrogen (2 amu, B) TPD from (*S*)-propylene oxide adsorbed on Pt(111) as a function of initial exposure. Two main molecular desorption peaks are seen, one at 195 K for the monolayer, which saturates after approximately 1.8 langmuirs, and a second at 145 K due to multilayer condensation starting at 2.0 langmuirs. A small amount of hydrogen desorption from propylene decomposition is seen at all coverages in two peaks about 370 and 480 K.

Figure 5B reports the TPD data for hydrogen production, the only other desorbing product detected in this system. The features at 145 and 195 K match those seen for molecular desorption, and correspond to cracking of the parent molecule in the mass spectrometer. The first and main hydrogen desorption peak assignable to the decomposition of adsorbed propylene oxide has an onset of about 320 K and peaks around 370 K, and a second broad peak is seen about 480 K. The total hydrogen yield is relatively low, and reaches its maximum at low

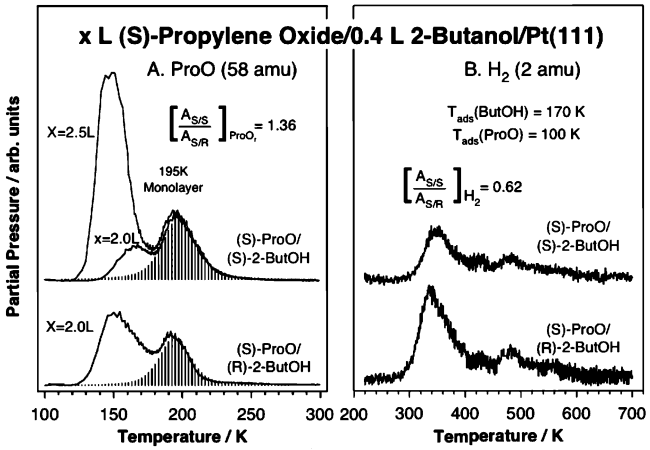

Figure 6. Propylene oxide (58 amu, A) and hydrogen (2 amu, B) TPD from titration experiments of 2-butoxide chiral layers with propylene oxide. The chiral 2-butoxide layers were prepared first by dosing 0.4 langmuirs of either (*R*)- (bottom) or (*S*)-2-butanol (top) on Pt(111) at 170 K. (*S*)-Propylene oxide was then adsorbed at 100 K, 2.0 langmuirs on the (*R*)-2-butoxide layer and either 2.0 or 2.5 langmuirs on the (*S*)-butoxide case. The data on the left indicate both a ~5 K higher desorption temperature and an increase of about 35% in (*S*)-propylene oxide uptake on the (*S*)-2-butoxide layer compared to the (*R*)-2-butoxide case. On the other hand, the right panel indicates a larger extent of decomposition in the latter system.

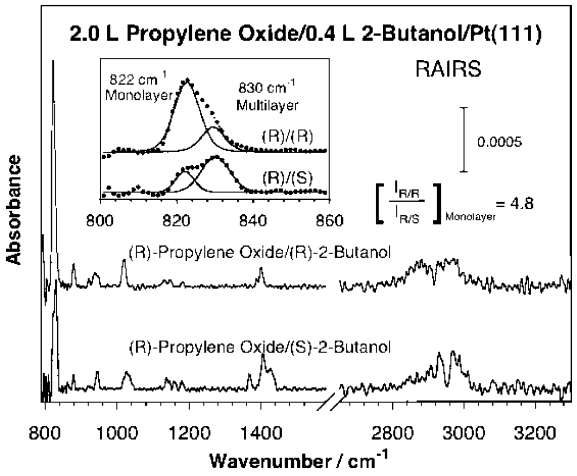

Figure 7. RAIRS from propylene oxide/2-butoxide chiral surfaces similar to those described in Figure 6, except that in this case the (*R*)- (top) and (*S*)-2-butoxide (bottom) layers were dosed with 2.0 langmuirs of (*R*)-propylene oxide instead. A number of differences are seen between the two spectra, in particular in the region corresponding to the ring deformation vibrational mode (shown in detail in the inset). Specifically, the peak at 822 cm^{-1} due to the monolayer is about five times more intense for the (*R*)-propylene oxide/(*R*)-2-butoxide case.

exposures, below 1.0 langmuirs. It appears that propylene oxide decomposition is inhibited by crowding of the surface.

3.3. Probing of 2-Butoxide Layers with Propylene Oxide. Having characterized independently the surface chemistry of 2-butanol and propylene oxide, it is now possible to characterize the chirality of 2-butoxide overlayers using propylene oxide as a probe molecule. This work relies on a few key observations from the chemistry reported above, namely: (1) the formation of 2-butoxide species on Pt(111) upon heating adsorbed 2-butanol to temperatures between approximately 170 and 200 K; (2) the higher molecular desorption temperature of propylene oxide from the first layer, as seen in the TPD traces at 195 K instead of 145 K, the temperature associated with the multilayer; (3) the clear differences in the IR spectra of the propylene oxide monolayer compared to those from the multilayer, in particular the shift in frequency seen in the ring deformation mode, δ_{oop}-(ring), from 830 to 822 cm^{-1}; (4) the inhibition of the propylene oxide decomposition on the surface at high coverages; and (5) the onsets of hydrogen production from 2-butoxide and propylene oxide decomposition at 300 and 320 K, respectively.

Figure 6 shows results from experiments designed to measure surface enantioselectivity using TPD. In these experiments, 0.4 langmuirs of either enantiopure (*R*)- (bottom traces) or enantiopure (*S*)- 2-butanol (top) were adsorbed on a Pt(111) surface at 170 K to produce a layer of the corresponding 2-butoxide chiral surface species. Those samples were subsequently saturated with enantiopure (*S*)-propylene oxide at 100 K, and the TPD data were then recorded. Figure 6A shows the traces obtained for molecular propylene oxide desorption. As in Figure 5, two peaks are seen at approximately 145 and 195 K, associated with the multilayer and monolayer, respectively. The key result here is the higher yield for monolayer desorption seen for the (*S*)-ProO/(*S*)-2-ButOH case (top trace), which amounts to approximately 1.36 times that seen with (*S*)-ProO/(*R*)-2-ButOH (bottom). This indicates a preference for adsorption of the same type of propylene oxide enantiomer used to make the butoxide chiral surface layer. It is also seen from these data that, for the same 2.0 langmuir exposure, the total propylene oxide yield (including both the monolayer and the multilayer) is higher with the (*S*)/(*R*) pair, but that can be easily explained by the increase in sticking coefficient upon transition from monolayer to multilayer adsorption (see above). A third experiment was carried out by dosing 2.5 langmuirs of (*S*)-ProO on the (*S*)-2-butoxide layer (second trace in top) to ensure that monolayer saturation was attained in this case. Indeed, the additional propylene oxide adsorbs in the multilayer, and the yield from the monolayer matches, within experimental error, that obtained with the 2.0 langmuirs dose.

Figure 6B reports the TPD traces obtained for hydrogen production. To interpret those results, it is worth noticing that the first H_2 desorption peak displays an onset of about 300 K. Given that propylene oxide decomposition starts above 320 K and that such decomposition may be inhibited by crowding of the surface (see above), we ascribe the hydrogen detected in these experiments to 2-butoxide decomposition. What is seen in these data is that significantly more decomposition takes place on the (*R*)-2-butoxide layer, approximately 50% more than on the (*S*)-2-butoxide case. This is an interesting observation, since no difference is seen between the two cases when adsorbed alone on the clean Pt(111) surface. Clearly, there is some synergy between the coadsorbed butoxide and propylene oxide species, an effect which persists upon heating to temperatures above those require to desorb the latter. It could be argued that the propylene oxide helps the reorganization of the butoxide layer into a better packed structure to allow for the enhanced coadsorption. The fact that the (*S*)/(*S*) butoxide/propylene oxide pair results in a higher ProO coverage suggests that the butoxide layer is better interlocked in that case, a fact that may inhibit its decomposition. In any case, what is clear is that the differences in decomposition yields must be related to differences in the interactions between the two coadsorbates upon variations in chiral pairing.

Figure 7 provides further evidence from RAIRS experiments corroborating the enantioselectivity of the adsorption of propylene oxide on 2-butoxide chiral surface layers. In this case 0.4 langmuirs of either (*R*)- (bottom trace) or (*S*)- 2-butanol (top) was again adsorbed on the Pt(111) surface at 170 K, but that was followed by low-temperature adsorption of (*R*)-

propylene oxide instead. The differences in monolayer and multilayer adsorption were in this case followed by the intensities of the vibrational band for the ring deformation, δ_{oop}(ring), at 822 and 830 cm^{-1}, respectively (data enlarged in the inset). A large difference is seen in the intensity of the signal for the monolayer, which is almost five times larger for the (*R*)/(*R*) pair compared to the (*R*)/(*S*) counterpart. The opposite is true for the multilayer, which is more clearly visible in the spectra for the (*S*)-2-butanol case both by the higher intensity of the 830 cm^{-1} mode and by the appearance of some of the other peaks (2970, 2935, 1440, 1369 cm^{-1}) associated with multilayer condensation. Again, it is clear that the 2-butoxide layer with the same chirality can provide more adsorption sites for the propylene oxide probe. On the other hand, this effect is not easy to quantify using the RAIRS data, because the vibrational signal intensities there are also affected by the orientation of the molecule. In fact, the differences in relative intensities seen between the two cases suggest different adsorption geometries for the propylene oxide. Specifically, the sharper and more intense peak for the methyl wagging mode, $\omega(CH_3)$, at 1020 cm^{-1} and the lower intensity of the methylene scissoring, $\gamma(CH_2)$, at 1401 cm^{-1} in the (*R*)/(*R*) layer (compared to the (*R*)/(*S*) case) points to a flatter adsorption. This also explains at least in part the higher intensity of the out-of-plane ring deformation peak, δ_{oop}(ring), of the monolayer at 822 cm^{-1}, and indicates that not only more propylene oxide adsorbs on the (*R*)/(*R*) homochiral surface, but that those molecules occupy a larger surface area.

4. Discussion

The TPD and RAIRS data reported here corroborate our main hypothesis, that the chiral layers formed by enantiopure 2-butanol on Pt(111) leave adsorption sites which display enantioselectivity toward the adsorption of chiral propylene oxide. In both Figures 6 and 7 evidence was provided for the preference for propylene oxide adsorption on surfaces with the same chirality. This is in qualitative agreement with the results reported previously by Tysoe et al. on Pd(111),[29] although the effect appears to be more pronounced in their case than ours. Moreover, our study adds a couple of finer points to this surface enantioselectivity picture. First, an effect induced by coadsorbed propylene oxide on the thermal chemistry of the chiral 2-butoxide surface layers was identified. It seems that the coadsorption system is somewhat dynamic and that the probing propylene oxide molecules induce a reorganization of the butoxide layer. Only a synergy between the alkoxide and the propylene oxide can explain the difference in reactivity between the (*R*)- and (*S*)-2-butoxide layers reported in the right panel of Figure 6. Second, the difference between the homochiral and heterochiral coadsorbed layers manifests itself not only as a difference in the extent of adsorption of propylene oxide on the 2-butoxide layers but also in changes in the adsorption geometry of the probe molecule. In fact, both effects work in concert, that is, the homologous (*R*)/(*R*) and (*S*)/(*S*) systems not only can pack more propylene oxide molecules but also in an adsorption configuration with a larger footprint. Finally, note that the (*S*)-propylene oxide monolayer desorbs at higher temperatures from (*S*)-2-butoxide (197 K) than from (*R*)-2-butoxide (193 K) layers (Figure 6A), suggesting a slightly stronger binding in the former case.

A broader question is how general the chiral effect reported here may be. Although no definitive answer can be provided to that query without further systematic studies with more surfaces and more molecules, a few pointers may be identified already. Perhaps the similar enantioselectivity seen for 2-butoxide on Pt(111) and Pd(111) can be justified in terms of the similar chemistry seen on both surfaces. In both cases, (1) butoxide species can be easily isolated upon thermal activation of adsorbed 2-butanol, (2) those butoxide intermediates undergo subsequent β-hydride elimination to butanone at higher temperatures, (3) propylene oxide displays significantly less surface reactivity, and (4) the ProO monolayer adsorbs strongly on the surface and can therefore be easily differentiated from the multilayer by both RAIRS and TPD. However, since all these characteristics may apply to other transition metal surfaces, perhaps more critical is the similar temperatures at which the transformations above are seen on platinum and palladium. There are some subtle differences between the two metals, such as the more complex high-temperature conversion seen for 2-butanol on Pt(111), but that seems to only affect the extent and not the fundamental nature of the chiral imprinting effect identified in these studies.

The question of the role of the nature of the substrate in defining chiral imprinting is critical in catalysis. Indeed, such a mechanism is believed to be responsible for the enantioselective hydrogenation of β-keto esters on nickel catalysts modified by tartaric acid.[21,22] Interestingly, it has not been easy to extend this idea to other reactants or catalysts. In terms of surface-science studies, Raval and co-workers have been able to demonstrate the formation of chiral superstructures by tartaric acid on Cu(110) surfaces,[25,48] but have run into some difficulties when trying to extend those results to Ni(110).[27,28] It is likely that the reactivity of the surface plays a role in defining the stability of such superstructures, but additional data will be required to develop a more detailed picture. Experiments have also been carried out to identify the molecular properties that help with such chiral behavior.[26,49] Recent experiments in Tysoe's laboratory have suggested that perhaps the templating chiral molecule needs two anchoring points to prevent it from rotating freely on the surface. They have looked into the chiral effect induced on Pd(111) by a number of alcohols, organic acid, and amino acids and reported some degree of enantioselectivity with most but not all of the molecules; significant exceptions were identified for 2-methylbutanoic acid, valine, and leucine. On the other hand, preliminary results from our laboratory suggest that 2-methylbutanoic acid does lead to a small but measurable enantioselectivity effect on Pt(111). Future experiments will help resolve these issues.

5. Conclusions

Temperature programmed desorption and reflection adsorption infrared spectroscopies were used to characterize the adsorption and surface chemistry of 2-butanol and propylene oxide on Pt(111). In the case of 2-butanol, monolayer bonding takes place through the oxygen atom and with the C−O bond close to perpendicular to the surface. Multilayers are easily condensed at liquid nitrogen temperatures and incur extensive hydrogen bonding. Thermal activation of 2-butanol monolayers leads to the formation of 2-butoxide surface groups around 170 K and subsequent conversion above 200 K. The main desorbing product in this case is butanone, which is produced via β-hydride elimination and detected about 270 K, but other molecules are seen as well, including ethane, ethylene, propanal, butanal, and butylene oxide. In terms of the adsorption of propylene oxide, the monolayer bonds through its oxygen atom and with the ring rotated to bring the methyl group close to the metal and somewhat tilted away from the surface normal. This interaction is quite strong, as manifested by both a 50 K increase in

desorption temperature compared with the multilayer and significant red shifts in the frequencies of the ring vibrational modes.

The adsorption of enantiopure 2-butanol on Pt(111) leads to the formation of chiral superstructures on the surface, as manifested by the preferential adsorption of propylene oxide with the same chirality as the underlying layer. In particular, according to TPD results, the (*S*)-2-butoxide layer produced by dosing 0.4 langmuirs of (*S*)-2-butanol at 170 K allows for the adsorption of approximately 35% more (*S*)-propylene oxide than the analogous (*R*)-2-butoxide layer. In turn, the propylene oxide in the homochiral system significantly inhibits further thermal decomposition of the butoxide species, presumably by forcing them in a well-packed structure with limited empty sites for dehydrogenation. The (*R*)-propylene oxide/(*R*)-2-butoxide system, which must display the same behavior as the (*S*)/(*S*) pair studied by TPD, was also used to determine (by RAIRS) that the propylene oxide adopts a different geometry, with the ring plane closer to parallel to the surface, in the homochiral pairing cases.

Acknowledgment. Funding for this research was provided by a grant from the U.S. Department of Energy.

References and Notes

(1) Addadi, L.; Weiner, S. *Nature* **2001**, *411*, 753.
(2) Francotte, E. *Chim. Nouv.* **1996**, *14*, 1541.
(3) Giancarlo, L. C.; Flynn, G. W. *Acc. Chem. Res.* **2000**, *33*, 491.
(4) Cai, Y.; Bernasek, S. L. *J. Am. Chem. Soc.* **2004**, *126*, 14234.
(5) Hazzazi, O. A.; Attard, G. A.; Wells, P. B. *J. Mol. Catal. A: Chem.* **2004**, *216*, 247.
(6) Baiker, A.; Blaser, H. U. In *Handbook of Hetrogeneous Catalysis*; Ertl, G., Knözinger, H., Weitkamp, J., Eds.; VCH: Weinheim, Germany, 1997; Vol. 4, pp 2422−2436.
(7) Orito, Y.; Imai, S.; Niwa, S.; Nguyen Gia, H. *Yuki Gosei Kagaku Kyokaishi* **1979**, *37*, 173.
(8) Tungler, A.; Kajtar, M.; Mathe, T.; Toth, G.; Fogassy, E.; Petro, J. *Catal. Today* **1989**, *5*, 159.
(9) Baiker, A. *J. Mol. Catal. A: Chem.* **1997**, *115*, 473.
(10) Wells, P. B.; Wilkinson, A. G. *Top. Catal.* **1998**, *5*, 39.
(11) LeBlond, C.; Wang, J.; Liu, J.; Andrews, A. T.; Sun, Y.-K. *J. Am. Chem. Soc.* **1999**, *121*, 4920.
(12) Bürgi, T.; Baiker, A. *J. Catal.* **2000**, *194*, 445.
(13) Vayner, G.; Houk, K. N.; Sun, Y.-K. *J. Am. Chem. Soc.* **2004**, *126*, 199.
(14) Kubota, J.; Zaera, F. *J. Am. Chem. Soc.* **2001**, *123*, 11115.
(15) Chu, W.; LeBlanc, R. J.; Williams, C. T.; Kubota, J.; Zaera, F. *J. Phys. Chem. B* **2003**, *107*, 14365.
(16) Ma, Z.; Kubota, J.; Zaera, F. *J. Catal.* **2003**, *219*, 404.
(17) Ma, Z.; Lee, I.; Kubota, J.; Zaera, F. *J. Mol. Catal. A: Chem.* **2004**, *216*, 199.
(18) Ma, Z.; Zaera, F. *J. Phys. Chem. B* **2005**, *109*, 406.
(19) Burgi, T.; Baiker, A. *Acc. Chem. Res.* **2004**, *37*, 909.
(20) LeBlanc, R. J.; Chu, W.; Williams, C. T. *J. Mol. Catal. A: Chem.* **2004**, *212*, 277.
(21) Hoek, A.; Sachtler, W. M. H. *J. Catal.* **1979**, *58*, 276.
(22) Izumi, Y. *Adv. Catal.* **1983**, *32*, 215.
(23) Webb, G.; Wells, P. B. *Catal. Today* **1992**, *12*, 319.
(24) Raval, R. *CATTECH* **2001**, *5*, 12.
(25) Ortega Lorenzo, M.; Haq, S.; Bertrams, T.; Murray, P.; Raval, R.; Baddeley, C. J. *J. Phys. Chem. B* **1999**, *103*, 10661.
(26) Humblot, V.; Barlow, S. M.; Raval, R. *Prog. Surf. Sci.* **2004**, *76*, 1.
(27) Humblot, V.; Haq, S.; Muryn, C.; Hofer, W. A.; Raval, R. *J. Am. Chem. Soc.* **2002**, *124*, 503.
(28) Humblot, V.; Haq, S.; Muryn, C.; Raval, R. *J. Catal.* **2004**, *228*, 130.
(29) Stacchiola, D.; Burkholder, L.; Tysoe, W. T. *J. Am. Chem. Soc.* **2002**, *124*, 8984.
(30) Tysoe, W. T. Personal communication.
(31) Hoffmann, H.; Griffiths, P. R.; Zaera, F. *Surf. Sci.* **1992**, *262*, 141.
(32) Janssens, T. V. W.; Zaera, F. *J. Catal.* **2002**, *208*, 345.
(33) Zaera, F.; Chrysostomou, D. *Surf. Sci.* **2000**, *457*, 89.
(34) Steininger, H.; Lehwald, S.; Ibach, H. *Surf. Sci.* **1982**, *123*, 264.
(35) Zaera, F. *Surf. Sci.* **1991**, *255*, 280.
(36) Socrates, G. *Infrared Characteristic Group Frequencies: Tables and Charts*, 2nd ed.; Wiley: Chichester, U.K., 1994.
(37) Quinan, J. R.; Wiberley, S. E. *Anal. Chem.* **1954**, *26*, 1762.
(38) Greenler, R. G. *J. Chem. Phys.* **1966**, *44*, 310.
(39) Zaera, F.; Hoffmann, H.; Griffiths, P. R. *J. Electron Spectrosc. Relat. Phenom.* **1990**, *54/55*, 705.
(40) Zaera, F. In *Encyclopedia of Chemical Physics and Physical Chemistry*; Moore, J. H., Spencer, N. D., Eds.; IOP: Philadelphia, PA, 2001; Vol. 2, pp 1563−1581.
(41) *Registry of Mass Spectral Data*; Stenhagen, E., Abrahamson, S., McLafferty, F., Eds.; Wiley-Interscience: New York, 1974.
(42) Xu, X.; Friend, C. M. *Surf. Sci.* **1992**, *260*, 14.
(43) Shekhar, R.; Barteau, M. A. *Catal. Lett.* **1995**, *31*, 221.
(44) Muhler, M. In *Handbook of Heterogeneous Catalysis*; Ertl, G., Knözinger, H., Weitkamp, J., Eds.; VCH: Weinheim, Germany, 1997; Vol. 5, pp 2274−2295.
(45) Zaera, F. *Catal. Today* **2002**, *81*, 149.
(46) Gleason, N.; Guevremont, J.; Zaera, F. *J. Phys. Chem. B* **2003**, *107*, 11133.
(47) Tobin, M. C. *Spectrochim. Acta* **1960**, *16*, 1108.
(48) Humblot, V.; Raval, R. *Appl. Surf. Sci.* **2005**, *241*, 150.
(49) Stacchiola, D.; Burkholder, L.; Zheng, T.; Weinert, M.; Tysoe, W. T. *J. Phys. Chem. B* **2005**, *109*, 851.